Polymer Integrated Waveguide Optical Biosensor by Using Spectral Splitting Effect

Xiaonan HAN[1], Xiuyou HAN[1*], Yuchen SHAO[1], Zhenlin WU[1], Yuxin LIANG[1,4],
Jie TENG[2], Shuhui BO[3], Geert MORTHIER[4], and Mingshan ZHAO[1]

[1]School of Physics and Optoelectronic Engineering, Dalian University of Technology, Dalian, 116024, China

[2]No. 38 Research Institute, China Electronics Technology Group Corporation, Hefei, 230088, China

[3]Technical Institute of Physics and Chemistry, Chinese Academy of Sciences, Beijing, 100190, China

[4]Photonics Research Group, Department of Information Technology, Ghent University-IMEC, 9000 Ghent, Belgium

*Corresponding author: Xiuyou HAN   E-mail: xyhan@dlut.edu.cn

Abstract: The polymer waveguide optical biosensor based on the Mach-Zehnder interferometer (MZI) by using spectral splitting effect is investigated. The MZI based biosensor has two unequal width sensing arms. With the different mode dispersion responses of the two-arm waveguides to the cladding refractive index change, the spectral splitting effect of the output interference spectrum is obtained, inducing a very high sensitivity. The influence of the different mode dispersions between the two-arm waveguides on the spectral splitting characteristic is analyzed. By choosing different lengths of the two unequal width sensing arms, the initial dip wavelength of the interference spectrum and the spectral splitting range can be controlled flexibly. The polymer waveguide optical biosensor is designed, and its sensing property is analyzed. The results show that the sensitivity of the polymer waveguide optical biosensor by using spectral splitting effect is as high as 10^4 nm/RIU, with an improvement of 2–3 orders of magnitude compared with the slot waveguide based microring biosensor.

Keywords: Optical biosensor; integrated waveguide; spectral splitting; sensitivity

1. Introduction

Integrated waveguide optical biosensors have broad applications in environmental monitoring, food safety, and healthcare with the advantages of the low cost, compact structure, real-time detection, and label-free sensing [1‒4]. Among various structures for integrated waveguide optical biosensors [5‒8], Mach-Zehnder interferometers (MZIs) have been attracting much attention due to their simple structure, easiness for fabrication. MZI based biosensors make use of the optical interference effect for sensing. When the phase difference between two arms is altered by the ambient analyte, the intensity or the resonant wavelength of the output interference signal changes, which reflects the information of the analyte, such as the kind or the concentration [9‒11].

The sensitivity of the MZI based integrated waveguide optical biosensor can be improved by increasing the cumulative amount of phase change. For example, in [12], the two arms of the MZI based

biosensor were set to be the spiral structure to increase the arm length. It increases the interaction distance between the analyte and lightwave, and improves the sensitivity. However, this structure increases the size of the biosensor. In [13], the sensing arm of the MZI based biosensor was set to be a slot waveguide structure to increase the interaction degree between the analyte and lightwave, aiming at obtaining large phase change. However, this approach increases the complexity of the waveguide design and the difficulty of the device fabrication.

In [14], the spectral splitting characteristic of the integrated waveguide interference structure was studied. If the phase difference between two optical paths satisfies a certain condition, there is a minimum power in the output spectrum at the dip wavelength, which is called as the critical wavelength. When the index of the analyte changes, the minimum power of the output spectrum is split into two dip wavelengths towards the opposite directions. The index change in the analyte can be determined by measuring the splitting wavelength, and then the information of the analyte is obtained. Because of the different mode dispersions of the two optical paths, a large splitting wavelength can be obtained with a small change of ambient refractive index, thus the very high sensitivity can be obtained. In [15], the silicon on the isolator (SOI) waveguide based MZI sensor with two unequal width arms was prepared. Laser irradiation was used to simulate the sensing process. The sensor could work at the critical wavelength by controlling the temperature, and the spectral splitting phenomenon was observed experimentally. In [16], the porous silicon based MZI sensor with two unequal width arms which worked at 1550 nm was simulated and analyzed. Different optical field distributions can be obtained since the two arms have different widths, thus the condition of spectral splitting can be satisfied. Because the position of the critical wavelength varies with the change in phase difference, the

different phase periods with different phase differences can be distinguished. It solves the phase-ambiguity problem of the interference sensors and increases the dynamic range of sensing. The basic principle of the interference spectrum is analyzed in above-mentioned literatures, and the spectrum splitting phenomenon has been observed experimentally. However, as far as we know, the optimal design of the biosensor structure with a controllable initial critical wavelength and a spectral splitting range to meet the practical sensing and interrogation applications haven't been reported in detail.

In this paper, the polymer waveguide MZI based biosensor by using the spectral splitting effect is investigated. The relationships between the phase difference and the cladding refractive indices or the length of the sensing arms are analyzed. The widths of the sensing arms are chosen properly to obtain a large phase difference and to realize the spectral splitting. For the practical sensing and interrogation applications, the two unequal width arms of the MZI are chosen to be different lengths. By adjusting the length difference, the initial critical wavelength of the interference spectrum can be designed flexibly, and the spectral splitting range can be controlled easily. The polymer waveguide MZI based biosensor fabricated by the micro-nano imprinting technique is designed. The results show that the controllable initial critical wavelength and spectral splitting range can be realized with the proposed sensing arm structure. Compared with the slot waveguide microring biosensor, the sensitivity of the spectral splitting based MZI biosensor can be enhanced by 2 to 3 orders of magnitude.

2. Operation principle

Figure 1 illustrates the structure of the spectral splitting based waveguide biosensor. It is mainly composed of two multimode interference (MMI) couplers and two sensing arms. The widths of the two sensing arms are unequal in order to obtain the

different mode dispersion responses to the refractive index change in the analyte. The MMI structure is adopted instead of the usual Y branch structure to split and combine the lightwave, which is helpful to reduce the transmission loss caused by the big Y branch angle and has a large tolerance to the imperfection of waveguide fabrication. Figure 2 shows the waveguides' cross section of the two sensing arms. Polymer Ormocore [17, 18] is used as the waveguide core, which is on the SiO_2 under the cladding. The biological sample under test, namely the analyte, covers both sensing arms, which avoids etching an extra sensing pool [19, 20]. Therefore, the complexity of the waveguide device fabrication is reduced, and the sensor array integration can be easily realized. The micro-nano imprinting technique is used to fabricate the polymer waveguide biosensor [21], thus the waveguide core may have the residual flat layer after demolding. The thickness of the residual flat layer is H_s. The structural parameters of the integrated waveguide biosensor are as follows: W_1 and W_2 are the waveguide widths of the sensing arms, H is the waveguide height, L_{arm1} and L_{arm2} are the longitudinal lengths of the two arms, G_1 and G_2 are the lateral spacings between one sensor arm and the straight waveguide of the MMI structure, l_1 and l_2 are the lengths of two bend waveguides, L_{bend} is the longitudinal length of the bend waveguides, L_{MMI} is the length of the MMI, W_{MMI} is the width of the MMI, D is the spacing between the two output straight waveguides of the MMI, and L_{taper} and W_{taper} are the length and width of the taper section, respectively.
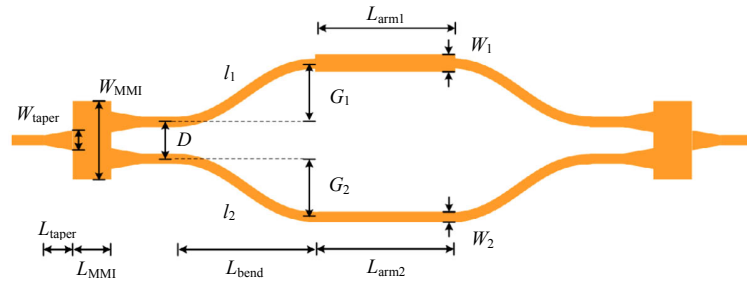

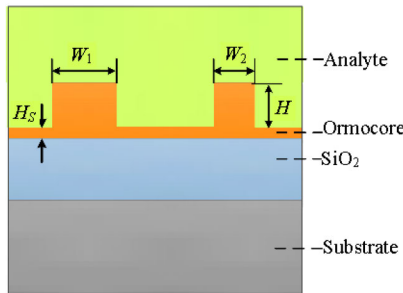Fig. 1 Structure of the waveguide biosensor with two unequal width arms.

Fig. 2 Waveguides' cross section of two sensing arms.

According to the optical interference principle of the MZI, the output power of the biosensor can be expressed as

$$P_{out} = 0.5 P_{in} \left(1 + \cos \Delta \varphi \right) \qquad (1)$$

where P_{in} and P_{out} are the input power and output power of the MZI based biosensor, respectively. The phase difference between the two sensing arms represented by $\Delta \varphi$ can be expressed as

$$\Delta \varphi = \frac{2\pi}{\lambda} L_{arm} \left(n_{eff1} - n_{eff2} \right) \qquad (2)$$

where L_{arm} is the length of each arm, assuming $L_{arm1} = L_{arm2} = L_{arm}$, and n_{eff1} and n_{eff2} are the effective refractive indices of the guided modes in the two sensing arms, respectively.

Figure 3 illustrates the spectral splitting principle of the interference biosensor. When the total phase difference between the two arms of the MZI based biosensor is an odd times of π, the output power will reach the minimum, which is shown as the curves with dot mark in Fig. 3. The corresponding wavelength is called the critical wavelength. When the refractive index of the upper cladding changes, the phase difference will change accordingly, then the output power at the critical wavelength will not be the minimum. The unique minimum power is

split into two dip wavelengths towards the opposite directions, which leads to the spectral splitting shown as the curves with triangle mark in Fig. 3. Due to the different mode dispersions of the guided modes in the two arms, the splitting wavelength can be very large with a small refractive index change in the upper cladding. As a result, the high sensitivity of the biosensor can be obtained.
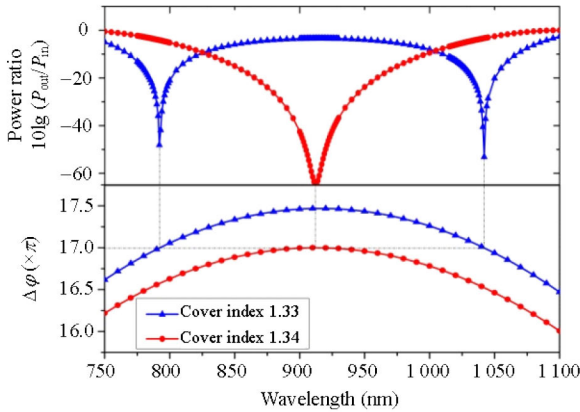

Fig. 3 Spectral splitting principle of the MZI based biosensor.

3. Biosensor structure design

According to the waveguides' cross section structure shown in Fig. 2, the finite difference beam propagation method (FD-BPM) is used to design the MZI waveguide biosensor structure. With the need to inject the phosphate buffer solution (PBS) in the microfluidic channel as the reference in the optical sensing applications [21], the PBS is chosen as the original material of the upper cladding in the analysis of waveguide. The transverse electric (TE) polarization state is chosen, and the refractive indices of each waveguide layer at 850 nm are as follows: upper cladding n_{PBS} =1.340, core n_{core} = 1.543, and lower cladding $n_{cladding}$ =1.453. With the micro-nano imprinting technique, the waveguide height H =1 μm and flat layer thickness H_s =0.2 μm are chosen.

According to the optical interference principle and spectral splitting characteristic, the effective refractive indices of the guided modes in the two sensing arms affect the phase difference directly.

The two sensing arms of the MZI based biosensor have different widths and only transmit the fundamental modes. The requirement of the single-mode condition for the waveguide width is analyzed. The effective refractive index with different waveguide widths is shown in Fig. 4, where Mode 0 means the fundamental mode and Mode 1 means the first-order guided mode. When the waveguide width is less than 1.5 μm, the single-mode condition is met. The narrow width will enhance the aspect ratio of waveguides' cross section, which increases the difficulty of the waveguide device preparation. So the widths of two arms are chosen as W_1=1.4 μm and W_2=1 μm, respectively.
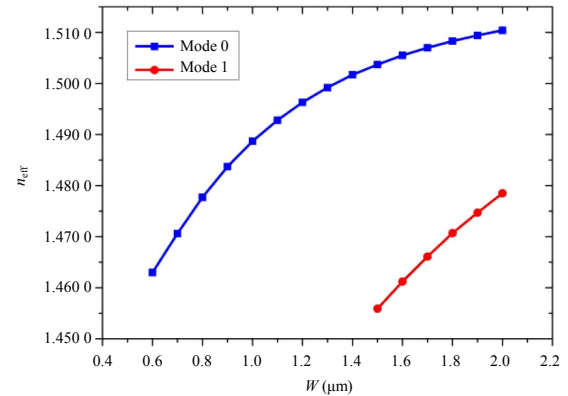

Fig. 4 Effective refractive index of the guided mode versus waveguide width.

Besides the effective refractive index of the arm waveguide, the lengths of sensing arms (L_{arm1} and L_{arm2} in Fig. 1) also affect the phase difference response greatly. When the lengths of two bend waveguides are equal ($l_1 = l_2$), the lengths of two sensing arms are also equal ($L_{arm1} = L_{arm2}$), and both are set to be 624 μm, then the total phase difference will be an odd times of π calculated with (2). The concentration change in the biological sample solution is simulated by changing the refractive index of upper cladding. Figure 5 shows the transmission spectrum of the biosensor. The dip shifts away from the critical wavelength in the opposite directions, thus the spectral splitting is obtained. We plan to use the super luminescent

diode (SLED, Fiberer Corp.) with a wavelength range of 820 nm – 860 nm in the subsequent experiment, that is to say, the detectable wavelength range is 820 nm – 860 nm. So the spectral splitting range due to the concentration change in the biological sample solution should be between 820 nm and 860 nm. According to Fig. 5, if we choose the left side of the splitting spectrum for sensing, the initial critical wavelength should be adjusted. The initial critical wavelength can be changed by altering the widths of two sensing arms. Because the adjustable range of the waveguide width is very small, the adjustive accuracy should be very high, which increases the difficulty of waveguide device fabrication. Here, two unequal length sensing arms are adopted, and the initial critical wavelength can be flexibly adjusted by changing the length difference.
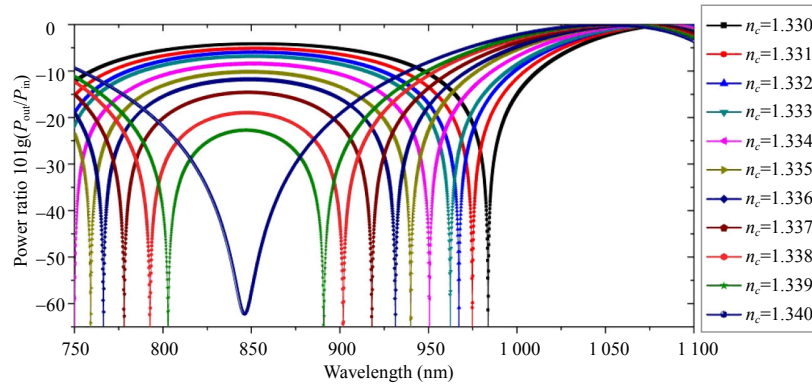

Fig. 5 Transmission spectrum under different indices of upper cladding ($L_{\text{arm1}} = L_{\text{arm2}} = 624\,\mu\text{m}$).

Figure 6 illustrates the modified biosensor structure with two unequal length sensing arms. The longitudinal lengths of both the two sensing arms are L_{arm}. The lateral spacing between the narrower arm and straight waveguide of the MMI structure is G_3. The narrow sensing arm consists of two identical bend waveguides, and the length of each section is $\sqrt{\left(G_3^2 + \left(L_{\text{arm}}/2\right)^2\right)}$. When the lengths of the two sensing arms are not equal, (1) can be expressed as

$$P_{\text{out}} = 0.5 P_{\text{in}}\left(1 + \cos\left(\Delta\varphi_w - \Delta\varphi_l\right)\right) \quad (3)$$

where $\Delta\varphi_w$ and $\Delta\varphi_l$ are the phase difference induced by the equal length of two arms and phase difference induced by the length difference between two arms, respectively.

$$\Delta\varphi_w = \frac{2\pi}{\lambda} L_{\text{arm}}\left(n_{\text{eff1}} - n_{\text{eff2}}\right) \quad (4)$$

$$\Delta\varphi_l = \frac{2\pi}{\lambda} n_{\text{eff2}}\Delta L \quad (5)$$

where ΔL is the length difference between two arms of the MZI biosensor:

$$\Delta L = 2\sqrt{\left(G_3^2 + \left(L_{\text{arm}}/2\right)^2\right)} - L_{\text{arm}}. \quad (6)$$
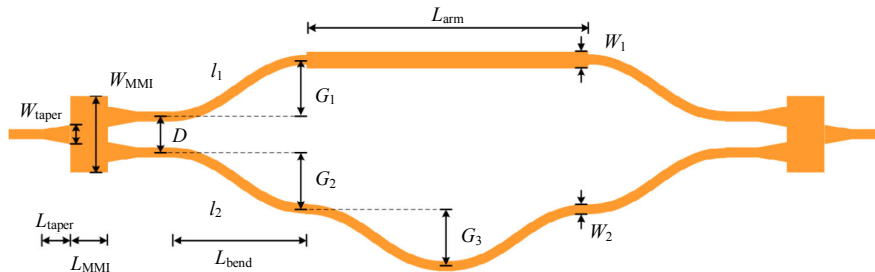

Fig. 6 Total structure of the modified biosensor with two unequal length arms.

According to (5), the splitting spectrum in the left of the critical wavelength can cover the wavelength range of 820 nm – 860 nm by setting an appropriate ΔL. ΔL can be obtained by adjusting L_{arm} and G_3. When $L_{\text{arm}} = 657\,\mu\text{m}$ and $G_3 = 17.1\,\mu\text{m}$, there is $\Delta L = 0.89\,\mu\text{m}$, and Figs. 7 and 8 show the power

transmission curves and phase difference curves, respectively. The spectrum corresponding to $n_{\text{cladding}} = 1.340$ will obtain the minimum power value

at the critical wavelength. And the left side of the splitting spectrum will cover the wavelength range of 820 nm–860 nm, which meets the design requirements.
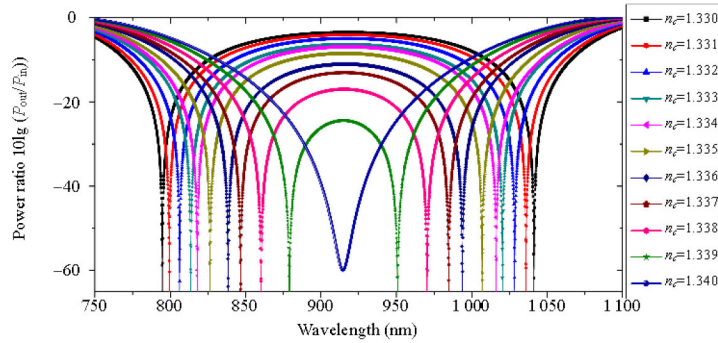

Fig. 7 Power transmission curves under different refractive indices of upper cladding ($L_{\text{arm}} = 657\,\mu\text{m}$ and $G_3 = 17.1\,\mu\text{m}$).
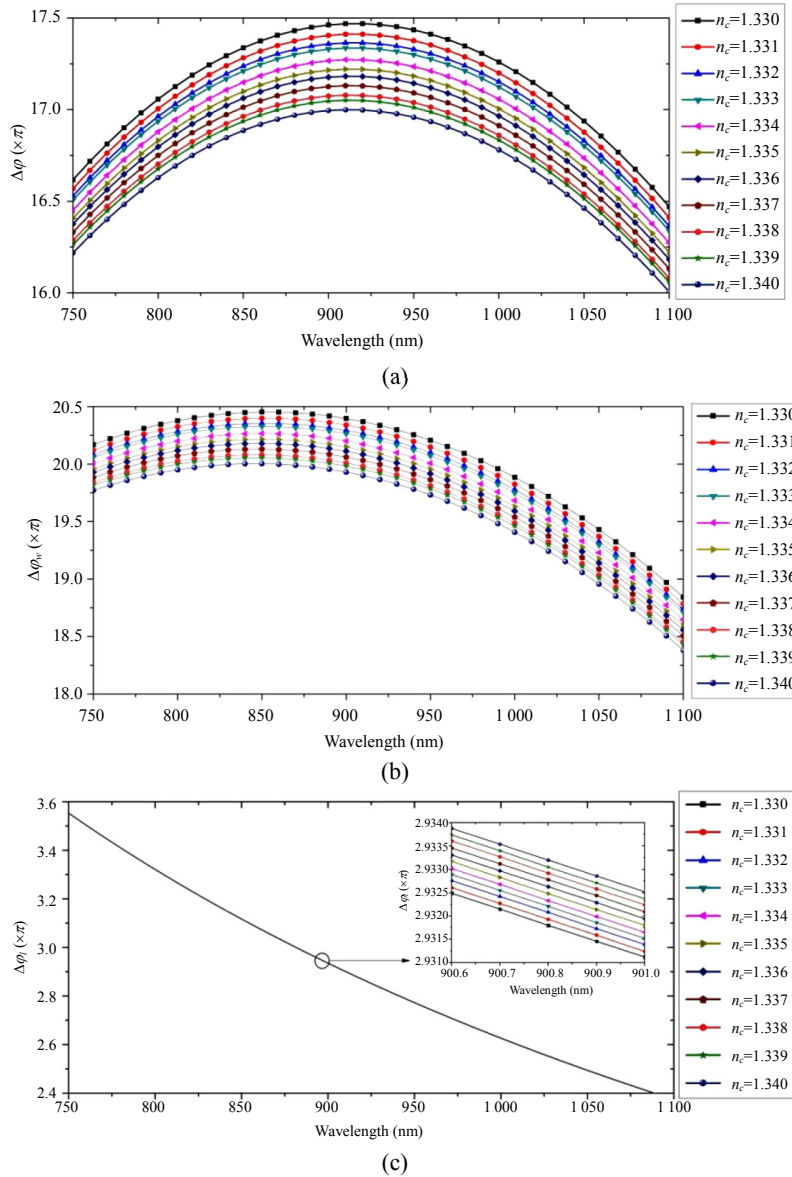

(a)

(b)

(c)

Fig. 8 Phase difference versus wavelength ($L_{\text{arm}} = 657\,\mu\text{m}$ and $G_3 = 17.1\,\mu\text{m}$): (a) total phase difference $\Delta\varphi$, (b) phase difference $\Delta\varphi_w$ induced by the equal length of two arms, and (c) phase difference $\Delta\varphi_l$ induced by the length difference between two arms.

The next is to design the MMI based coupler. Figure 9 illustrates the MMI waveguide structure. The MMI structure is designed from the viewpoint of reducing the insertion loss. According to the principle of self-imaging of the MMI structure [22, 23], the optimized structural parameters of the MMI are as follows: the width of the MMI structure is $W_{MMI} = 9\,\mu m$, the length of the MMI structure is $L_{MMI} = 74\,\mu m$, the spacing between two output straight waveguides is $D = 4.6\,\mu m$, the length of the taper section is $L_{taper} = 62\,\mu m$, and the width of the taper section is $W_{taper} = 2.2\,\mu m$. Figure 10 shows the power transmission of the MMI based coupler. The output power of both arms is 49.3%, corresponding to the extra insertion loss of each arm of 0.07 dB. Finally, the optimized structural parameters of the MZI based biosensor are as follows: $H = 1\,\mu m$, $H_s = 0.2\,\mu m$, $W_1 = 1.4\,\mu m$, $W_2 = 1\,\mu m$, $G_1 = G_2 = 3\,\mu m$, $G_3 = 17.1\,\mu m$, $L_{arm} = 657\,\mu m$, $L_{bend} = 100\,\mu m$, $L_{taper} = 62\,\mu m$, $W_{taper} = 2.2\,\mu m$, $D = 4.6\,\mu m$, $W_{MMI} = 9\,\mu m$, $L_{MMI} = 74\,\mu m$.
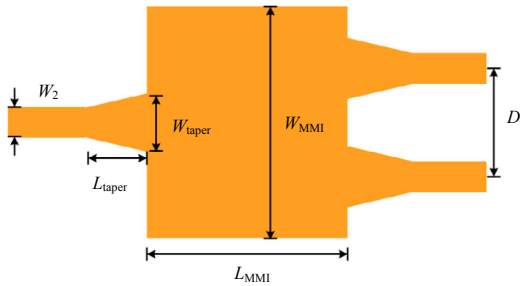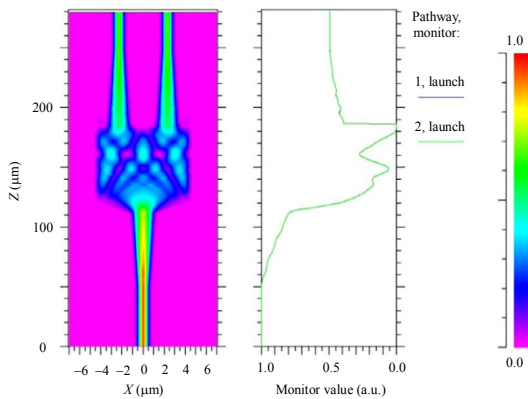

Fig. 9 Structure of the MMI waveguide.

Fig. 10 Field distribution of the optical wave in the MMI waveguide structure.

4. Sensitivity analysis

From Fig. 7, it can be seen that the critical wavelength with the cladding refractive index of 1.34 is 912 nm, which is not within the range of the detectable wavelength 820 nm – 860 nm from the SLED. Because the wavelength difference between the shifted dip wavelength and critical wavelength is too large with a small upper cladding index change, the left dip wavelength of the splitting spectrum with the cladding index of 1.339 is set as the reference to determine the sensitivity of the MZI based biosensor for the practical interrogation. In Fig. 7, the splitting spectrum value $\Delta\lambda$, namely the wavelength difference between the shifted dip wavelength with different cladding refractive indices and reference dip wavelength with the cladding index of 1.339 can be obtained, and the data are listed in Table 1. According to Table 1, the sensitivity of the MZI biosensor with spectral splitting is about 10^4 nm/RIU, which is improved by 2 – 3 orders of magnitude compared with the slot waveguide microring sensor [24]. The relationship curve between the cladding index variation and spectral splitting value is plotted in Fig. 11. By fitting the curve of Fig. 11 with polynomial, the relationship equation can be obtained as (7). According to (7), the analyte refractive index variation Δn_c can be obtained by the measured splitting spectrum value $\Delta\lambda$.
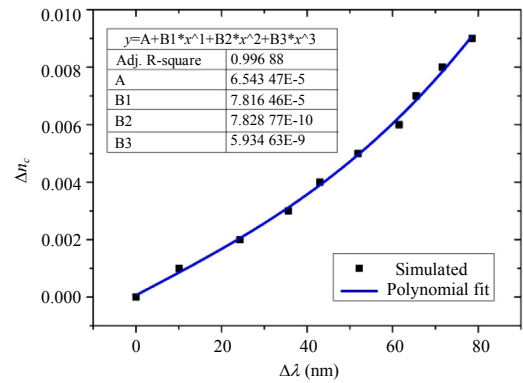

Fig. 11 Upper cladding refractive index variation versus splitting spectrum value.

$$\Delta n_c = 5.93463 \times 10^{-9} \Delta\lambda^3 + 7.82877 \times 10^{-1}\ \Delta\lambda^2 + 7.81646 \times 10^{-5} \Delta\lambda + 6.54347 \times 10^{-5} \qquad (7)$$

Table 1 Spectral splitting value and ratio between the spectral splitting value and upper cladding index change.

n_c	1.33	1.331	1.332	1.333	1.334	1.335	1.336	1.337	1.338	1.339
$\Delta\lambda$ (nm)	78.6	71.6	65.5	61.5	51.9	43.0	35.6	24.3	10.1	0.0
$\Delta\lambda/\Delta n_c$ ($\times 10^4$ nm/RIU)	0.87	0.90	0.94	1.03	1.04	1.08	1.19	1.22	1.01	

5. Conclusions

In this paper, the polymer waveguide optical biosensor based on the MZI structure by using spectral splitting effect has been investigated. With the different mode dispersion responses of the guided modes in the two unequal width waveguides, the high sensitivity can be achieved by properly choosing the waveguide widths of the two sensing arms. In order to meet the requirement of the practical sensing and interrogation application, the two sensing arms with different lengths are chosen. By adjusting the length difference between the two sensing arms, the initial critical wavelength and splitting spectrum range can be controlled easily. The polymer waveguide biosensor with the micro-nano imprinting technique is designed, and the sensing property is analyzed. The results show that the sensitivity of the polymer waveguide biosensor as high as 10^4 nm/RIU can be achieved.

Acknowledgment

References

[1] A. L. Washburn and R. C. Bailey, "Photonics-on-a-chip: recent advances in integrated waveguides as enabling detection elements for real-world, lab-on-a-chip biosensing applications," *Analyst*, 2011, 136(2): 227‒236.

[2] V. J. Cadarso, A. Llobera, M. Puyol, and H. Schift, "Integrated photonic nanofences: combining subwavelength waveguides with an enhanced evanescent field for sensing applications," *ACS Nano*, 2016, 10(1): 778‒785.

[3] L. G. Carrascosa, C. S. Huertas, and L. M. Lechuga, "Prospects of optical biosensors for emerging label-free RNA analysis," *Trac Trends in Analytical Chemistry*, 2016, 80: 177‒189.

[4] E. Makarona, P. Petrou, S. Kakabakos, K. Misiakos, and I. Raptis, "Point-of-need bioanalytics based on planar optical interferometry," *Biotechnology Advances*, 2016, 34(3): 209‒233.

[5] X. Fan, I. M. White, S. I. Shopova, H. Zhu, J. D. Suter, and Y. Sun, "Sensitive optical biosensors for unlabeled targets: a review," *Analytica Chimica Acta*, 2008, 620(1‒2): 8‒26.

[6] H. N. Daghestani and B. W. Day, "Theory and applications of surface plasmon resonance, resonant mirror, resonant waveguide grating, and dual polarization interferometry biosensors," *Sensors*, 2010, 10(11): 9630‒9646.

[7] M. Sathish and S. Talabattula, "Polarization analysis of an asymmetrically etched rib waveguide coupler for sensing applications," *Photonic Sensors*, 2013, 3(2): 178‒183.

[8] J. H. Zhang, F. S. Chen, B. Sun, and K. X. Chen, "Integrated optical waveguide sensor for lighting impulse electric field measurement," *Photonic Sensors*, 2014, 4(3): 215‒219.

[9] Z. Qi, N. Matsuda, K. Itoh, M. Murabayashi, and C. R. Lavers, "A design for improving the sensitivity of a Mach-Zehnder interferometer to chemical and biological measurands," *Sensors and Actuators B: Chemical*, 2002, 81(2‒3), 254‒258.

[10] S. Dante, D. Duval, B. Sepúlveda, A. B. González-Guerrero, J. R. Sendra, and L. M. Lechuga, "All-optical phase modulation for integrated interferometric biosensors," *Optics Express*, 2012, 20(7): 7195‒7205.

[11] T. F. Yang, "Optimal design and fabrication of polymeric planar optical waveguide bio-chemical sensor," Ph.D. dissertation, Jilin University, Jilin, 2014.

[12] A. Densmore, D. X. Xu, S. Janz, P. Waldron, T. Mischki, G. Lopinski, *et al.*, "Spiral-path high-sensitivity silicon photonic wire molecular sensor with temperature-independent response," *Optics Letters*, 2008, 33(6): 596‒598.

[13] Q. Liu, X. Tu, K. W. Kim, J. S. Kee, Y. Shin, K. Han, *et al.*, "Highly sensitive Mach-Zehnder interferometer biosensor based on silicon nitride slot waveguide," *Sensors and Actuators B: Chemical*, 2013, 188(11): 681‒688.

[14] R. Levy and S. Ruschin, "Critical sensitivity in hetero-modal interferometric sensor using spectral interrogation," *Optics Express*, 2008, 16(25): 20516‒20521.

[15] R. Levy, S. Ruschin, and D. Goldring, "Critical sensitivity effect in an interferometer sensor," *Optics Letters*, 2009, 34(19): 3023‒3025.

[16] T. Hutter, S. R. Elliott, and S. Ruschin, "Dynamic range enhancement and phase-ambiguity elimination in wavelength-interrogated interferometric sensor," *Sensors and Actuators B: Chemical*, 2013, 178(3): 593‒597.

[17] Ormocore Products, Micro Resist Technol. GmbH, Berlin, Germany, 2014.

[18] R. Morarescu, P. K. Pal, X. Han, M. Zhao, P. Bienstman, and G. Morthier, "Polymer microring resonators for biosensing applications by nanoimprint lithography," in *The 17th International Conference on Transparent Optical Networks*, Hungary, Sept. 5‒9, pp. 1‒4, 2015.

[19] R. Bruck, E. Melnik, P. Muellner, R. Hainberger, and M. Lämmerhofer, "Integrated polymer-based Mach-Zehnder interferometer label-free streptavidin biosensor compatible with injection molding," *Biosensors and Bioelectronics*, 2011, 26(9): 3832‒3837.

[20] B. Sepúlveda, J. S. D. Río, M. Moreno, F. J. Blanco, K. Mayora, C. Domínguez, *et al.*, "Optical biosensor microsystems based on the integration of highly sensitive Mach-Zehnder interferometer devices," *Journal of Optics A: Pure and Applied Optics*, 2006, 8(7): S561‒S566.

[21] L. H. Wang, J. Ren, X. Y. Han, T. Claes, X. G. Jian, P. Bienstman, *et al.*, "A label-free optical biosensor built on a low-cost polymer platform," *IEEE Photonics Journal*, 2012, 4(3): 920‒930.

[22] L. B. Soldano and E. C. M. Pennings, "Optical multi-mode interference devices based on self-imaging: principles and applications," *Journal of Lightwave Technology*, 1995, 13(4): 615‒627.

[23] Y. C. Shao, X. Y. Han, X. N. Han, Z. L. Lu, Z. L. Wu, J. Teng, *et al.*, "Optimal design of 850 nm 2×2 multimode interference polymer waveguide coupler by imprint technique," *Photonic Sensors*, 2016, 6(3): 234‒242.

[24] X. N. Han, X. Y. Han, Y. C. Shao, Z. L. Lu, J. Teng, Z. L. Wu, *et al.*, "Study on polymer microring optical biosensor based on slot waveguide," *Acta Optical Sinica*, 2016, 38(4): 04130011‒04130018.